Elsevier Editorial System(tm) for Applied Numerical Mathematics

Manuscript Draft

Manuscript Number:

Title: A Domain Decomposition Method For Conservation Laws with Discontinuous Flux Function

Article Type: Research paper

Section/Category:

Keywords: Domain Decomposition Method; Conservation Laws with Discontinuous Flux Function; Nonoscillatory Scheme

Corresponding Author: Michael Herty,

Corresponding Author's Institution: TU Kaiserslautern

First Author: Michael Herty

Order of Authors: Michael Herty; Mohammed Seaid; Anita K Singh

Manuscript Region of Origin:

Abstract:

A Domain Decomposition Method For Conservation Laws with Discontinuous Flux Function

Michael Herty* Mohammed Seaïd* Anita K. Singh*

Abstract

A domain decomposition method for scalar conservation laws with discontinuous flux function is presented. The spatial domain is decomposed in subdomains at the location of the discontinuity of the flux function. The associated conservation law for each subdomain having then a continuous flux function is solved using a nonoscillatory relaxation scheme. Special coupling conditions at the subdomain interfaces are developed based on the direction of traveling waves. This method uses similar techniques recently used to treat junctions in network problems. The numerical performance of the method is illustrated on typical one-dimensional test examples like traffic models or two-phase flows.

Keywords. Domain Decomposition Method; Conservation Laws with Discontinuous Flux Function; Nonoscillatory Scheme

1 Introduction

Conservation laws with discontinuous flux function occur in many physical applications, for example in porous media flows [7], sedimentation phenomena [6], resonant models [10, 14] and vehicular traffic flows [23]. The development of efficient solution procedure for such problems is challenging, since in many applications its solution involves abrupt changes in flow variables at discontinuities. Standard numerical methods often perform badly on conservation laws with discontinuous flux function due to the presence of critical regions of high spatial activity such as shocks, boundary layers, wavefronts, pulses, etc. The present solution either oscillates wildly in the vicinity of such regions if the mesh is too coarse, or the fronts are smeared if too much dissipation is added to control the oscillations. Theoretical results can be found for example in [13, 22] among others. Recently, there has been a lot of interest in the numerical treatment of discontinuous flux functions for hyperbolic equations, see for example [12, 21]. We present an alternative view on those problems by introducing a domain decomposition procedure [19, 15, 8]. Our approach is inspired from recent work on partial differential equation on network geometries, see for example [9, 4, 1], and therefore coupling conditions for the subdomains are similar to the coupling conditions at the vertices of a network model.

*Fachbereich Mathematik, Technische Universität Kaiserslautern, D–67663 Kaiserslautern, Germany. E-mails: {herty,seaid,singh}@mathematik.uni-kl.de

The numerical solution of the conservation laws in subdomains with continuous flux function is carried out using a nonoscillatory relaxation scheme. Relaxation methods for hyperbolic equations of conservation laws have initially been introduced in [11]. The methods consist on replacing the original conservation law by a semilinear hyperbolic system with linear characteristic variables and a relaxation source term which rapidly takes the relaxation variable to the flux function when the relaxation time becomes small. The main advantages of relaxation methods are the semilinear construction of the approximating system and a special time implicit-explicit splitting for the relaxation term. The first advantage allows us to solve the system numerically without introducing Riemann solvers and the second avoids the solution of nonlinear system of algebraic equations. In fact, relaxation schemes are a combination of nonoscillatory upwind space discretization and a TVD implicit-explicit time integration of the resulting semi-discrete system, see for instance [11, 2, 3, 20, 21].

To examine the performance of the proposed domain decomposition procedure, we present numerical results on test examples related to traffic and two-phase flows. The obtained results demonstrate good shock resolution with high accuracy in smooth regions and without any nonphysical oscillations near the shock areas. From a practical point of view, the performance of the proposed domain decomposition method is very attractive since the computed solutions remain, stable, monotone and highly accurate even on coarse meshes without solving Riemann problems or requiring special front tracking techniques.

The structure of this paper is as follows. Section 2 formulates the domain decomposition method for scalar equations of conservation laws with discontinuous flux functions. Numerical solution of the sub-equations with continuous flux functions is briefly discussed in section 3. Section 4 presents numerical results and examples. Conclusions summarizing the paper are given in section 5.

2 A Domain Decomposition Method

We consider a scalar conservation law

$$\begin{aligned} \partial_t u + \partial_x f\,(x,u) &= 0, \qquad (x,t) \in \mathbb{R} \times \mathbb{R}^+, \\ u(x,0) &= u_0(x), \quad x \in \mathbb{R}, \end{aligned} \tag{2.1}$$

where the flux function $f(x,u)$ is piecewise differentiable and possibly has a finite number of discontinuities located at $\{x_1, \ldots, x_M\}$. We assume that on each spatial region $[x_m, x_{m+1})$ the function $(x,u) \longrightarrow f(x,u)$ is independent of the spatial variable x and strictly concave with single maximum. The assumptions on the flux function are motivated by examples on traffic flow models where, at certain location points x_m, a construction site or a lane reduction starts and continuous until the next location point x_{m+1} on the road. In the traffic flow terminology, these discontinuity points are know by junctions and a traffic road can contain more than one junction conducting to the notion of networks. The restriction to this (special) class of flux functions allows for a short presentation of the main ideas. However, the whole method can be applied to far more general flux functions and we also present later on numerical results on general discontinuous flux function. An example of a flux function under consideration is depicted in figure 1.

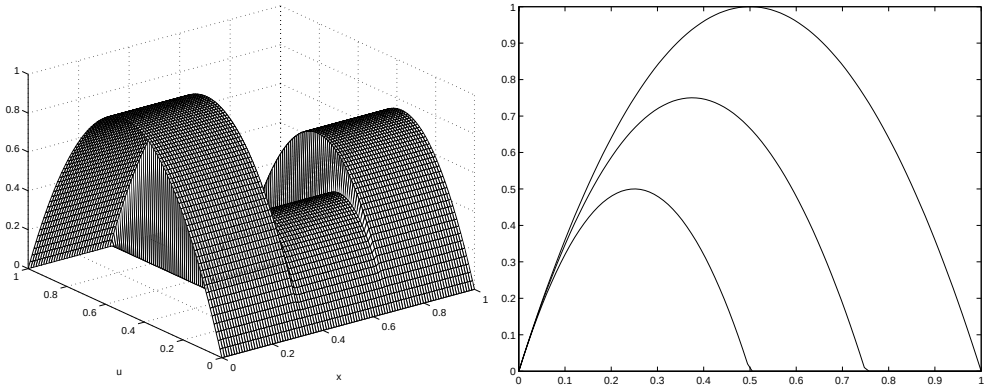

Figure 1: Flux function $f(x,u)$ with two discontinuities located at $x_1 = 1/3$ and $x_2 = 2/3$ being piecewise concave (right plot) and its interpretation as a network with three independent flux functions (left plot) where the arcs of the network are connected at x_i.

The basic idea of our approach is to apply a domain decomposition method to the problem (2.1). Thus, we decompose the spatial domain in a non-overlapping subdomains $\Omega_m = [x_m, x_{m+1})$ such that

$$\bigcup_{m=0}^{M} \Omega_m = \mathbb{R}, \qquad \Omega_k \cap \Omega_m = \emptyset, \quad \text{for} \quad k \neq m.$$

Hence, the problem (2.1) reduces to a sequence of M scalar conservation laws

$$\begin{aligned} \partial_t u_m + \partial_x f_m(u_m) &= 0, \qquad (x,t) \in \Omega_m \times \mathbb{R}^+, \\ u_m(x,0) &= u_0(x), \quad x \in \Omega_m, \end{aligned} \tag{2.2}$$

where the flux function $f_m(u)$ is defined by $f_m(u) = f(x,u)$ for $x \in \Omega_m$. It is clear that the flux function in (2.2) is a continuous function. Note that the subdomains Ω_1 and Ω_M are extended to $-\infty$ and $+\infty$, respectively. Boundary conditions necessary for the numerical solution of (2.2) on each subdomain Ω_m are given by the coupling conditions introduced below.

Once the solutions u_m of the conservation laws (2.2) are obtained, the solution of the original problem (2.1) is recovered by prolongation as

$$u(x,t) = u_m(x,t), \qquad (x,t) \in \Omega_m \times \mathbb{R}^+.$$

This approach has the advantage that each single conservation law is well-posed and can be solved by standard numerical methods designed for conservation laws with continuous flux functions. A special attention has to be given to the coupling conditions at the interfaces. We remark that, the domain decomposition procedure can also be seen as a network problem with a particular simple geometry and different flux functions f_m on each arc, see for example [9, 4]. Here, coupling conditions are derived, as in reference [9], from the weak formulation of the decomposed problems (2.2) as follows:

Consider a set of test functions $\{\phi_m\}_{m=1}^M$ with $\phi_m : \quad \Omega_m \times [0,+\infty] \longrightarrow \mathbb{R}$ having compact support in Ω_m and, for all $t \in \mathbb{R}^+$, satisfying the following conditions

$$\begin{aligned} \phi_m(x_m,t) &= \phi_{m+1}(x_m,t), \\ \partial_x\phi_m(x_m,t) &= \partial_x\phi_{m+1}(x_m,t), \qquad \forall\, m = 1,\dots,M-1. \end{aligned} \tag{2.3}$$

Let u be a weak solution to the problem (2.1) and let ψ be an arbitrary test function, $\psi \in C_0^\infty(\mathbb{R}\times\mathbb{R}^+)$. It is easy to verify that the functions ϕ_m defined as the restriction of ψ on Ω_m, *i.e.*

$$\phi_m(x,t) = \psi(x,t), \qquad (x,t) \in \Omega_m \times \mathbb{R}^+,$$

satisfy the conditions (2.3). Similarly, the restricted solution $u_m := u\big|_{\Omega_m\times\mathbb{R}^+}$ solves the conservation law (2.2) and the weak formulation for (2.1) yields

$$\begin{aligned} &\int_0^\infty \int_{\mathbb{R}} \partial_t\psi u + \partial_x\psi f(x,u)dxdt + \int_{\mathbb{R}} \psi(x,0)u_0(x)dx = \\ &\quad \sum_{m=1}^M \left(\int_0^\infty \int_{\Omega_m} \partial_t\phi_m u_m + \partial_x\phi_m f_m(u_m)dx + \int_{\Omega_m} \phi_m u_0(x)dx \right) = 0. \end{aligned} \tag{2.4}$$

If we require (2.4) for all sets of test functions $\{\phi_m\}_{m=1}^M$ with the property (2.3) and if each u_m is sufficiently regular, then the Rankine-Hugenoit jump conditions hold for all $t \in \mathbb{R}^+$:

$$f_m\left(u_m\left(x_m^-,t\right)\right) = f_{m+1}\left(u_{m+1}(x_m^+,t)\right), \qquad m = 1,\dots,M-1. \tag{2.5}$$

Note that conditions (2.5) are the appropriate coupling conditions which will be used to define boundary values for (2.2). For convenience, we give a brief derivation using a different motivation and notation than those presented in [9].

For each single subdomain Ω_m we consider the Riemann problems associated with the problem (2.2) at the boundary points $\hat{x}$ of Ω_m and defined as

$$\begin{aligned} \partial_t u_m + \partial_x f_m(u_m) &= 0, \qquad (x,t) \in \Omega_m \times \mathbb{R}^+, \\ u_m(x,0) &= \begin{cases} u^-, & \text{if} \quad x < \hat{x}, \\ u^+, & \text{if} \quad x > \hat{x}. \end{cases} \end{aligned} \tag{2.6}$$

The Riemann data is defined for $t = 0$ depending on the left boundary $\hat{x} = x_m$ or the right boundary $\hat{x} = x_{m+1}$ as

$$\begin{cases} u^- = u_0(x), & \text{if} \quad \hat{x} = x_{m+1}, \\ u^+ = u_0(x), & \text{if} \quad \hat{x} = x_m. \end{cases} \tag{2.7}$$

An (entropy) solution of (2.4) can be constructed such that all generated waves have locally non-positive $\hat{x} = x_{m+1}$ and non-negative $\hat{x} = x_m$ speed, respectively. Moreover, all solutions u_m satisfy the condition (2.5) for $x = x_m$ and $x = x_{m+1}$. The previous discussion holds true for all kinds of flux function. For simplicity of the presentation we now consider only concave flux functions $f_m : \; u \longrightarrow f_m(u)$. Then, the assumptions on the speed of the waves can be reformulated more explicitly by using the notion of demand and supply functions, compare [16]. In the sequel, we assume that the

concave flux functions f_m additionally satisfy $f_m(0) = 0$ and $f_m(u_{m,\max}) = 0$ for some value $u_{m,\max} > 0$, and the unique single maximum is reached at $u = \sigma_m$. Then, the demand function $d_m : u \longrightarrow d_m(u)$ corresponds the non-decreasing part of f_m *i.e.*,

$$d_m(u) := \begin{cases} f_m(u), & \text{if} \quad u \leq \sigma_m, \\ f_m(\sigma_m), & \text{otherwise.} \end{cases}$$

Analogously, the supply function $s_m : u \longrightarrow s_m(u)$ corresponds to the non-increasing part of the flux function f_m *i.e.*,

$$s_m(u) := \begin{cases} f_m(\sigma_m), & \text{if} \quad u \leq \sigma_m, \\ f_m(u), & \text{otherwise.} \end{cases}$$

Using the demand/supply functions we can easily characterize the Riemann data $u^{\pm}$ in (2.7), which gives rise to waves of positive or negative speeds.

Remark 2.1 *The concept of demand and supply functions can be extended to functions which are neither convex nor concave, see for example [5]. Then, the similar statements as in (2.1) and (2.2) is much more involved.*

Lemma 2.1 *Consider the problem (2.6) with a flux function satisfying the above assumptions and let the constant initial data u^- be given. Assume a flux function q is given such that*

$$0 \leq q < d_m(u^-).$$

Then, there exist a unique state u^+, such that the Riemann problem (2.6) admits only waves of non-negative speed. In addition, if $q = d_m(u^-)$ then we set $u^+ = u^-$ and the solution to (2.6) is constant. □

Proof: This proof is standard and the two possible cases are:

(i) If $u^- < \sigma_m$ then $d(u_m) = f_m(u_m)$. Thus, by the concavity of the flux function, there exists a point $\tau(u^-) > \sigma_m$ such that $f_m(\tau(u^-)) = f_m(u^-)$. Now, since f_m is continuous and strictly concave, there exists a unique state $u^+ \in [\tau(u^-), u_{m,\max}]$ such that $f_m(u^+) = q$. Moreover, the solution to (2.6) with data u^- and u^+ is a shock wave of negative speed.

(ii) If $u^- > \sigma_m$, then $d(u_m) = f_m(\sigma_m)$. Thus, there exists a unique state $u^+ \in [\sigma_m, u_{m,\max}]$ such that $f_m(u^+) = q$. Moreover, the solution to (2.6) is a rarefaction wave of negative speed if $u^+ < u^-$ and a shock wave elsewhere.

■

Lemma 2.2 *Consider the problem (2.6) with a flux function satisfying the above assumptions and let the constant initial data u^+ be given. Assume a flux q is given such that*

$$0 \leq q < s_m(u^+).$$

Then, there exists a unique state u^- such that the Riemann problem (2.6) admits only waves of non-positive speed. In addition, if $q = s_m(u^+)$ then we set $u^- = u^+$ and the solution to (2.6) is constant.

■

The proof is similar to the one of Lemma 2.1 and we omit the details. By virtue of Lemma 2.1 and Lemma 2.2 we are in a position to describe a solution to (2.4) and (2.1) satisfying the coupling conditions (2.5).

For brevity, assume that the flux function $f(x,u)$ in (2.1) has a single discontinuity located at the point $x = x_m$. Hence, the proposed domain decomposition method lead to two problems (2.2) to be solved in subdomains Ω_{m-1} and Ω_m. Let also assume that (at least locally) constant initial data $u_0(x) = u_k^0$ for $x \in \Omega_k$, $k \in \{m-1, m\}$ and with possibly different flux functions $f_{m-1} \neq f_m$. Then, the theorem below describes the admissible solutions u_{m-1} and u_m satisfying (2.5) and (2.2).

Theorem 2.1 *Consider the problems (2.2) in subdomains Ω_{m-1} and Ω_m with constant initial data $u_0(x) = u_{m-1}^0$ and $u_0(x) = u_m^0$ for $x \in \Omega_{m-1}$ and $x \in \Omega_m$, respectively. Then, there exists unique solutions $u_{m-1}(x,t)$ and $u_m(x,t)$ of the Riemann problems at the junction (2.6) and (2.7) with the following properties:*

(i) The solution $u_k(x,t)$ is a weak solution of the network problem (2.2) for $k \in \{m-1, m\}$ (and also to (2.4)). Furthermore, the condition (2.5) is satisfied.

(ii) The flux value $u_m(x_m^-, t)$ is maximal at the interface. □

Proof: Let $q := \min(d_{m-1}(u_{m-1}^0), s_m(u_m^0))$ be the flux at the interface $x = x_m$. Then, due to Lemma 2.1, there exists an admissible state $\bar{u}_{m-1}$ such that $f_{m-1}(\bar{u}_{m-1}) = q$. Furthermore, the solution to the Riemann problem (2.6) with initial data $u^- = u_{m-1}^0$ and $u^+ = \bar{u}_{i-1}$ is either constant or it consists of waves of non-positive speed only. Therefore, $u_{m-1}(x_m^-, t) = q$ for all $t \in \mathbb{R}^+$.

Similarly, due to Lemma 2.2, there exists an admissible state $\bar{u}_m$, such that $f_m(\bar{u}_m) = q$ and the solution to the Riemann problem (2.6) with initial data $u^- = \bar{u}_m$ and $u^+ = u_m^0$ is either constant or consists of waves non-positive speed. Therefore, $u_m(x_m^+, t) = q = u_{m-1}(x_m^-, t)$. Since q is defined as minimum of supply and demand functions, the flux is maximal at the interface $x = x_m$. This ends the proof. ■

Note that Theorem 2.1 describes admissible boundary values for a numerical procedure. A piecewise constant approximation u_m^n of u_m on Ω_m has to be supplemented with boundary conditions for example at $x = x_m$. The correct values to prescribe at $x = x_m$ are given by the states $u_m^{n+1} = \bar{u}_m$ of (2.1). Similarly, the approximation u_{m-1}^n is supplemented with the boundary conditions at $x = x_m$ given by $\bar{u}_{m-1}$. If there is more than one discontinuity in the flux function $f(x,u)$, then the above has to be repeated at each single discontinuity point. These hold for first-order methods only and is implemented in the numerical approach below.

Remark 2.2 *Obviously, if the flux function $f(x,u)$ is independent of x, the above discussion yields the entropy solution for a standard Riemann problem with initial data given by*

$$u(x,t) = \begin{cases} u^-, & \text{if} \quad x < x_m, \\ u^+, & \text{if} \quad x > x_m. \end{cases}$$

3 Nonoscillatory Discretization of Conservation Laws

To numerically solve the conservation laws (2.2) we consider the well established relaxation methods [11, 2]. We briefly present some implementation details, since the method below can also be applied to discontinuous flux functions without any change, compare [21].

Let consider a single equation in conservation laws (2.2)

$$\begin{aligned} \partial_t U + \partial_x F(U) &= 0, && (x,t) \in \Omega \times \mathbb{R}^+, \\ U(\hat{x},t) &= \hat{u}(t), && t \in \mathbb{R}_+, \\ U(x,0) &= u_0(x), && x \in \Omega, \end{aligned} \tag{3.1}$$

where U, F, Ω and $\hat{x}$ refer respectively, to any variable u_m, flux function f_m, subdomain Ω_m and junction point x_m in (2.2) with $m = 1, \ldots, M$. A relaxation approximation of equations (3.1) reads

$$\begin{aligned} \partial_t U + \partial_x V &= 0, \\ \partial_t V + \lambda \partial_x U &= -\frac{1}{\varepsilon}\Big(V - F(U)\Big), \\ U(\hat{x},t) = \hat{u}(t), &\qquad V(\hat{x},t) = F\left(\hat{u}(t)\right), \\ U(x,0) = u_0(x), &\qquad V(x,0) = F\left(u_0(x)\right), \end{aligned} \tag{3.2}$$

where ε is the relaxation rate and V is a relaxation variable expected to converge to $F(U)$ as ε approaches zero. The parameter λ is the characteristic speed selected based on the *sub-characteristic* condition [11],

$$\frac{|\partial_U F(U)|}{\sqrt{\lambda}} \leq 1. \tag{3.3}$$

As stated in the introduction, the main advantage of numerically solving the relaxation system (3.2) over the original conservation law (3.1) lies in the special structure of the linear characteristic fields and localized lower order terms. Indeed, the linear hyperbolic nature of (3.2) makes it possible to approximate its solution easily by underresolved stable numerical discretization that uses neither Riemann solvers spatially nor nonlinear system of algebraic equations solvers temporally.

As in many kinetic models, the relaxation system (3.2) can be reformulated in diagonalizable form

$$\begin{aligned} \partial_t \mathcal{F} + \sqrt{\lambda}\partial_x \mathcal{F} &= -\frac{1}{\varepsilon}\left(\mathcal{F} - \hat{\mathcal{F}}\right), \\ \partial_t \mathcal{G} - \sqrt{\lambda}\partial_x \mathcal{G} &= -\frac{1}{\varepsilon}\left(\mathcal{G} - \hat{\mathcal{G}}\right), \end{aligned} \tag{3.4}$$

where the kinetic variables (Riemann invariants) $\mathcal{F}$ and $\mathcal{G}$ are defined as

$$U = \mathcal{F} + \mathcal{G}, \qquad V = \sqrt{\lambda}(\mathcal{F} - \mathcal{G}). \tag{3.5}$$

The local equilibrium functions (Maxwellians) $\hat{\mathcal{F}}$ and $\hat{\mathcal{G}}$ are given by

$$\hat{\mathcal{F}} = \frac{U}{2} + \frac{F(U)}{2\sqrt{\lambda}}, \qquad \hat{\mathcal{G}} = \frac{U}{2} - \frac{F(U)}{2\sqrt{\lambda}}.$$

Note that, the systems (3.4) and (3.2) are equivalent such that a discretization of each one of them lead essentially to discretization of the other. For spatial discretization, we consider control volumes $[x_{i-1/2}, x_{i+1/2}]$ with uniform dimension $\Delta x = x_{i+1/2} - x_{i-1/2}$. Integrating (3.2) with respect to x over the control volume and keeping the time t continuous we obtain the following semi-discrete system

$$\begin{aligned} \frac{dU_i}{dt} + \mathcal{D}_x V_i &= 0, \\ \frac{dV_i}{dt} + \lambda_i \mathcal{D}_x U_i &= -\frac{1}{\varepsilon}\left(V_i - F(U_i)\right), \end{aligned} \tag{3.6}$$

where $\Psi_i(t)$, is the space average of a generic solution Ψ ($\Psi = U$ or $\Psi = V$) in the cell $[x_{i-1/2}, x_{i+1/2}]$ at time t,

$$\Psi_i(t) = \frac{1}{\Delta x}\int_{x_{i-1/2}}^{x_{i+1/2}} \Psi(x,t)dx.$$

The difference notation $\mathcal{D}_x$ in (3.6) is defined as

$$\mathcal{D}_x \Psi_i = \frac{\Psi_{i+1/2} - \Psi_{i-1/2}}{\Delta x},$$

where $\Psi_{i\pm1/2} = \psi(x_{i\pm1/2}, t)$ are the numerical fluxes at $x = x_{i\pm1/2}$. Since $\mathcal{F}$ and $\mathcal{G}$ travel along constant characteristics with speed $+\lambda$ and $-\lambda$, respectively, upwind reconstructions can be easily applied to them. For example, a first-order upwind scheme yields

$$\mathcal{F}_{i+1/2} = \mathcal{F}_i, \qquad \mathcal{G}_{i+1/2} = \mathcal{G}_{i+1}. \tag{3.7}$$

A second-order discretization can be reconstructed by incorporating limiters in (3.7). Using the Sweby's notation, the second-order reconstruction reads

$$\mathcal{F}_{i+1/2} = \mathcal{F}_i + \frac{1}{2}\Delta x \sigma_i^+, \qquad \mathcal{G}_{i+1/2} = \mathcal{G}_{i+1} + \frac{1}{2}\Delta x \sigma_{i+1}^-, \tag{3.8}$$

where σ_i^+ and σ_i^- are the slope of $\mathcal{F}$ and $\mathcal{G}$ on the cell $[x_{i-1/2}, x_{i+1/2}]$, respectively. For $\Psi^+ = \mathcal{F}$ and $\Psi^- = \mathcal{G}$, the slopes $\sigma^\pm$ are defined by

$$\sigma_i^\pm = \frac{1}{\Delta x}\left(\Psi_{i+1}^\pm - \Psi_i^\pm\right)\Phi(\theta_i^\pm), \qquad \theta_i^\pm = \frac{\Psi_i^\pm - \Psi_{i-1}^\pm}{\Psi_{i+1}^\pm - \Psi_i^\pm},$$

with $\Phi(\theta)$ defines the van Leer's slope limiter function

$$\Phi(\theta) = \frac{|\theta| + \theta}{1 + |\theta|}.$$

Once $\mathcal{F}_{i+1/2}$ and $\mathcal{G}_{i+1/2}$ are reconstructed using (3.7) or (3.8), the numerical fluxes $U_{i+1/2}$ and $V_{i+1/2}$ in the relaxation system (3.6) are obtained from (3.5) as

$$U_{i+1/2} = \mathcal{F}_{i+1/2} + \mathcal{G}_{i+1/2} \qquad \text{and} \qquad V_{i+1/2} = \sqrt{\lambda_i}(\mathcal{F}_{i+1/2} - \mathcal{G}_{i+1/2}).$$

Note that higher order discretization are also applicable. For instance, a third-order reconstruction for numerical fluxes in (3.6) based on essentially non-oscillatory method

has been studied in [2, 3, 21]. Recently a fifth-order reconstruction has been developed in [2] combining relaxation method with a weighted essentially non-oscillatory reconstruction.

Most relaxation schemes integrate the equation (3.6) in time using the implicit-explicit (IMEX) methods, compare [11, 2, 21] among others. In fact, the special structure of the nonlinear terms in (3.6) makes it trivial to evolve the flux terms explicitly and the source term implicitly. At the limit ($\varepsilon \longrightarrow 0$), the IMEX methods for (3.2) reduced to an explicit time integration of the original conservation law (3.1) based on the explicit scheme in IMEX methods. In this paper, for simplicity in presentation, we formulate only the relaxed scheme ($\varepsilon = 0$). Therefore, with Δt being the time step and Ψ^n denoting the approximate solution of a function Ψ at $t = n\Delta t$, the implementation of a second-order relaxed scheme to solve (3.6) can be carried out in the two following steps:

$$\begin{aligned} U_i^* &= U_i^n - \Delta t \mathcal{D}_x V_i^n \Big|_{V_i^n = F(U_i^n)}, \\ U_i^{**} &= U_i^* - \Delta t \mathcal{D}_x V_i^* \Big|_{V_i^* = F(U_i^*)}, \\ U_i^{n+1} &= \frac{1}{2}(U_i^n + U_i^{**}). \end{aligned} \tag{3.9}$$

It is worth remarking that, since the advective part in (3.6) is treated explicitly, the time stepping (3.9) is conditionally stable such as the time step Δt has to satisfy the CFL condition

$$\text{CFL} = \max_i \lambda_i \frac{\Delta t}{\Delta x} \leq 1, \tag{3.10}$$

Remark 3.1 *In general, the characteristic speeds λ_i can be chosen large enough such that the sub-characteristic condition (3.3) is satisfied. However, the numerical diffusion increases with their values and for accuracy reasons λ_i should be chosen as small as possible. throughout all the results presented in this paper, the characteristic speeds in (3.6) are calculated locally in each control volume and at each time step as*

$$\lambda_i = \max\left\{ \left|\partial_U F\left(U_{i-1/2}\right)\right|^2, \left|\partial_U F\left(U_{i+1/2}\right)\right|^2 \right\} + \tau, \tag{3.11}$$

where τ is a safety parameter set to 0.1 *for all examples to avoid that λ_i vanishes. For more discussions on the selection of characteristic speeds in general relaxation methods we refer to [2, 3, 20, 11].*

For completeness, we present the complete domain decomposition type algorithm for solving the equation (2.1). It consists of the following steps:

1. Decompose the spatial domain into a finite sequence of subdomains $\Omega_m = [x_m, x_{m+1})$, $m = 1, \ldots, M$, using the location points x_m of the discontinuity in the flux function.
2. For $m = 1, \ldots, M$:
   - **i.** Reconstruct the boundary values at x_m and x_{m+1} according to the coupling conditions (2.3).

ii. Solve the sub-equations of conservation laws with continuous flux functions in Ω_m using the numerical procedure described above.

3. Update the numerical solution u of (2.1) using the sub-solution u_m in Ω_m.

Note that, steps 2 and 3 have to be carry out at each time step in the computational process. We should point out that the DDM algorithm proposed in this paper differs from the canonical DDM methods used for elliptic partial differential equation in the fact that no iterations are required for resolving the interfaces.

4 Results and Numerical Examples

In this section we investigate numerically the performance of the proposed domain decomposition method. To this end we apply the method to several test examples on conservation laws with discontinuous flux functions. As a comparison, together with the new method, we have considered the relaxation schemes presented in [21], which were recommended by the authors. Here DDM, RELAX1 and RELAX2 stand respectively, for the domain decomposition method presented in section 3, the standard first-order relaxation and second-order relaxation schemes presented in [21]. In all our computations the CFL number is fixed to 0.75 and time steps Δt are calculated according to the condition (3.10).

4.1 Accuracy Test Example

This example consists of the equations (2.1) where the flux function is defined as

$$f(x,u) = k(x)u(1-u), \qquad k(x) = \begin{cases} 2, & \text{if} \quad 0 \le x \le 2.5, \\ \frac{25-2x}{10}, & \text{if} \quad 2.5 < x < 7.5, \\ 1, & \text{if} \quad 7.5 \le x \le 10, \end{cases} \tag{4.1}$$

with an initial condition given by

$$u_0(x) = \begin{cases} 0.9, & \text{if} \quad 0 \le x \le 2.5, \\ \frac{1+\sqrt{0.28}}{2}, & \text{if} \quad 2.5 < x \le 10. \end{cases} \tag{4.2}$$

It is easy to verify that the problem (4.1)-(4.2) has an exact steady-state solution defined as

$$u_\infty(x) = \begin{cases} 0.9, & \text{if} \quad 0 \le x \le 2.5, \\ \dfrac{1}{2} + \dfrac{\sqrt{k(x)^2 - 0.72k(x)}}{2k(x)}, & \text{if} \quad 2.5 < x < 7.5, \\ \frac{1+\sqrt{0.28}}{2}, & \text{if} \quad 7.5 \le x \le 10. \end{cases}$$

This exact steady-state solution can be used to quantify the results obtained by our DDM method in terms of some error norms. According to the proposed DDM method, the flux function (4.1) results in three subproblems to be solved with continuous flux functions. We have computed the approximate solution at $t = 10$. At this time

the approximated solutions are almost stationary, and therefore error norms can be calculated. We consider the L^∞- and L^1-error norms defined as

$$\max_{1\le i\le N} |u_i - u_\infty(x_i)| \qquad \text{and} \qquad \sum_{i=1}^{N} |u_i - u_\infty(x_i)|\,\Delta x, \tag{4.3}$$

respectively. Here, u_i and $u_\infty(x_i)$ are respectively, the computed and exact steady-state solutions at gridpoint x_i, whereas N denotes the number of gridpoints used in the spatial discretization. Table 1 lists the obtained error-norms using different values of N. It is clear that increasing the number of gridpoints in the spatial domain turns into a decrease of the error-norms in the computed solution. The proposed DDM method preserves the correct asymptotic accuracy.

Table 1: Error-norms for the accuracy test example.

N	L^∞-error	L^1-error
100	1.79e-3	4.25e-3
200	9.03e-4	2.08e-3
400	4.52e-4	1.03e-3
800	2.26e-4	5.12e-4
1600	1.13e-4	2.56e-4

In figure 2, we plot the computed steady-state solution using $N = 200$. For comparison we have included the results obtained using RELAX1 and RELAX2. Note that the exact steady-state solution is not included in this figure because it overlaps those obtained using DDM and RELAX2 methods. As can be seen, there is no significant differences in the resolutions of DDM and RELAX2 schemes. However, the RELAX1 scheme failed to accurately resolve the steady-state solution. Compare the location of the shock obtained using RELAX1 in figure 2. The DDM method performed well for this test example.

4.2 Traffic Flow Example

In this example we assess the performance of the proposed DDM method for traffic flow models. By taking into account the nature of vehicular roads, these models offer a realistic one-dimensional conservation law with discontinuous coefficient entries. The well-known Lighthill-Whitham and Richards model [17] for traffic flows can be written in conservation form as (2.1) where $u(x,t) = a(x)\rho(x,t)$ with $a(x)$ and $\rho(t,x)$ are the lane number and the density per-lane, respectively. The flux function is

$$f(x,u) = \frac{v(x)}{v_{max}} u(1-u), \tag{4.4}$$

where $v(x)$ is the free flow velocity at the point x and $v_{max} = \max_{x\in\mathbb{R}} v(x)$ is the maximum speed. Here, we examine the accuracy of DDM method for a bottleneck situation in traffic flow.

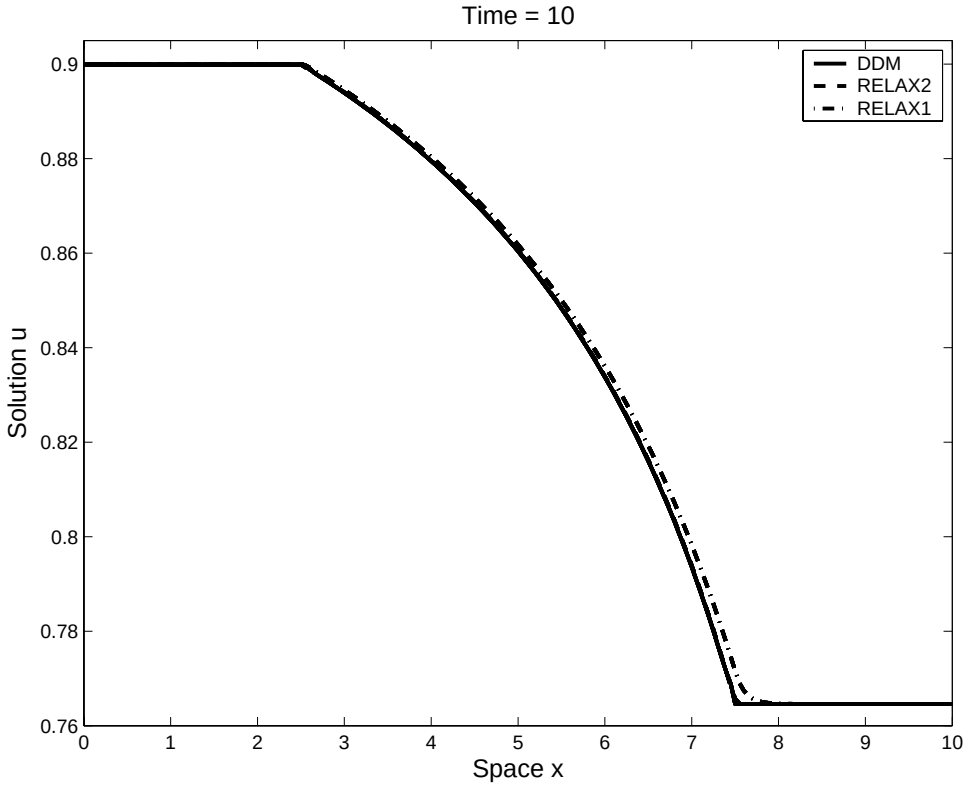

Figure 2: Results obtained for the accuracy test example.

We consider a road of length $L = 10\ Km$ with an initial density $\rho(x) = 0.2\ veh/Km$. The coefficients $a(x)$ and $v(x)$ are discontinuous functions given by

$$a(x) = \begin{cases} 4, & \text{if} \quad x < 3\ Km, \\ 2, & \text{if} \quad x \geq 3\ Km, \end{cases}, \qquad v(x) = \begin{cases} 1, & \text{if} \quad x < 3\ Km, \\ 0.6, & \text{if} \quad x \geq 3\ Km. \end{cases} \tag{4.5}$$

The DDM method applied to the equations (4.4)-(4.5) yields two subproblems to be solved in the roads $[0, 3)$ and $(3, 10]$ with continuous flux functions. In our computations, the total road is divided into 100 gridpoints and the duration of the simulation is 900 s. In figure 3 we display the results using dimensionless space x/L and dimensionless time tv_{max}/L. As expected, the RELAX1 scheme introduces extensive numerical dissipation in the computed solution, the RELAX2 scheme performs better but still diffusive effects are presented in its resolution. This numerical dissipation is substantially eliminated in the DDM results and the high accuracy of DDM method over the other relaxation schemes is clearly demonstrated.

4.3 Two-Phase Flow Example

As already mentioned in Remark 2.1, the proposed domain decomposition method can also be applied if the flux function on each subdomain is neither convex nor concave. The standard example of such situation is the Buckley-Leverett flux function. The Buckley-Leverett equation has serve as one of the simplest model of two-phase flow in

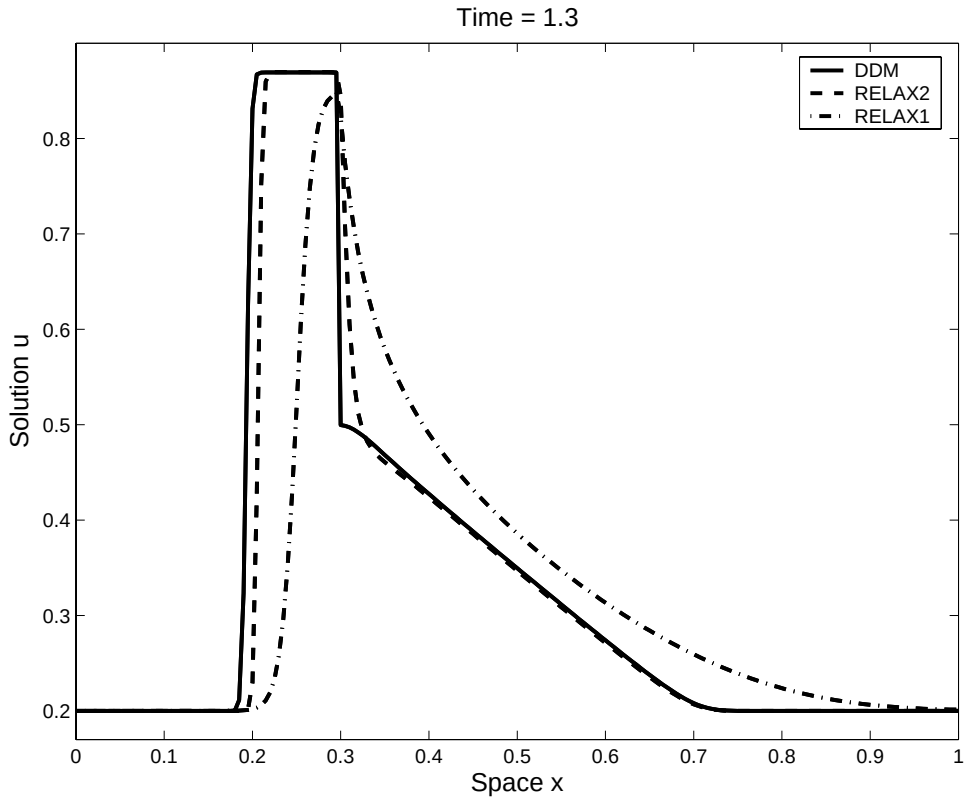

Figure 3: Results obtained for the example on traffic flow model.

a porous medium [18]. Here, the governing equations are given by (2.1) with

$$f(k(x),u) = \frac{u^2}{u^2 + k(x)(1-u)^2}, \qquad k(x) = \begin{cases} 50, & \text{if} \quad 0 \le x < 0.5, \\ 5, & \text{if} \quad 0.5 \le x \le 1. \end{cases} \tag{4.6}$$

The initial condition is

$$u_0(x) = \begin{cases} 0, & \text{if} \quad 0 \le x \le 1 - \frac{1}{\sqrt{2}}, \\ 1, & \text{if} \quad 1 - \frac{1}{\sqrt{2}} \le x \le 1. \end{cases}$$

Again, the DDM procedure decomposes this test example in two subproblems with continuous flux functions to be solved in the sub-intervals $[0, 0.5)$ and $(0.5, 1]$. Here, the total spatial domain is discretized into 200 gridpoints and the computed results are presented at $t = 0.2$.

Figure 4 shows the results computed using DDM, RELAX1 and RELAX2 schemes. As can be seen, the results obtained by the DDM method are more accurate than those obtained using the other relaxation schemes. The results again show very good performance of the DDM method for this test example.

5 Conclusions

In this paper, we constructed and studied a class of domain decomposition method for numerical solution of conservation laws with discontinuous flux functions. This

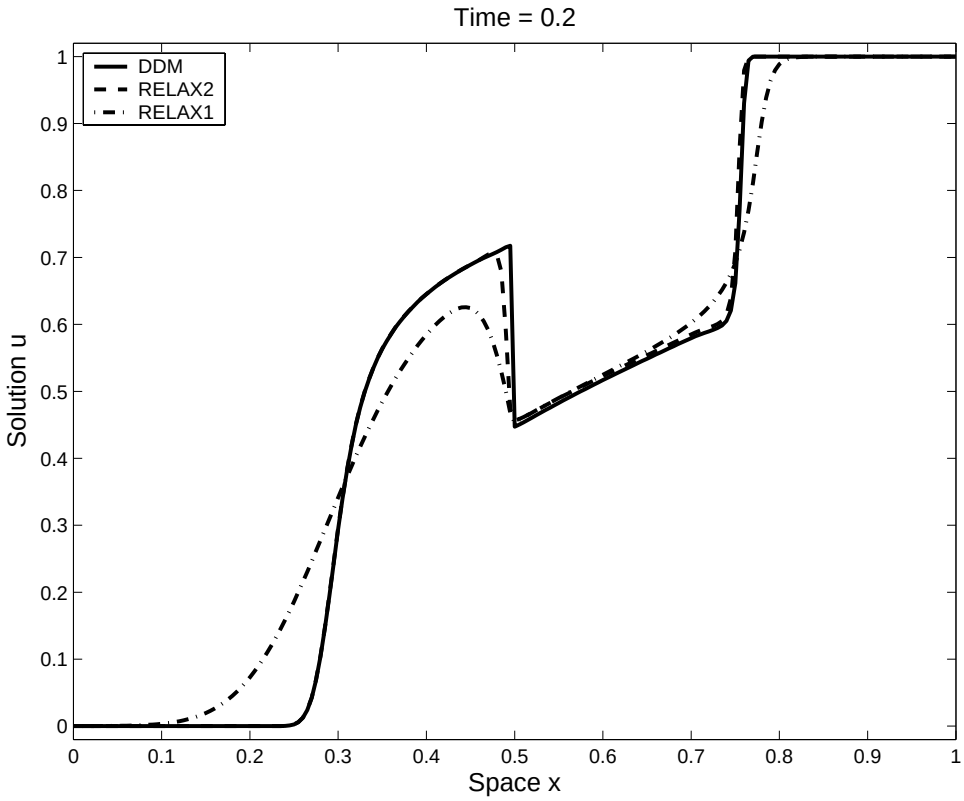

Figure 4: Results obtained for the example on two-phase flow model.

method is effective when the flux functions present more than one discontinuity within the same spatial domain. The main idea is to transform the problem at hand into a finite sequence of conservation laws with continuous flux functions easy to solve using conventional discretizations. We established the coupling conditions for the boundary interfaces. Similar procedure has been used in network problems. The performance of the proposed method has been illustrated in several test examples on conservation laws with discontinuous flux functions. Comparisons to the second-order relaxations scheme has also been presented in this paper. We find that the domain decomposition method is clearly superior to the other scheme. The performance of our method is very attractive since the computed solution remains stable, monotone and highly accurate even on coarse grids without requiring special front tracking procedures.

For systems of conservation laws, the principle of domain decomposition techniques can still be used, however, a different construction of coupling conditions at the interfaces is needed. In addition, the same ideas can also be extended to two-dimensional equations of conservation laws with discontinuous flux functions such as Euler equations in gas dynamics with heterogeneous thermodynamical properties. It is also a worthwhile subject to extend it for multi-phase flows in porous media. Currently, we are exploring the domain decomposition methods in these more general applications.

Acknowledgements. This work has been supported by the Kaiserslautern Excellence Cluster Dependable Systems and Mathematical Modelling.

References

[1] M. K. Banda, M. Herty, and A. Klar, *Coupling Conditions for Gas Networks Governed by the Isothermal Euler Equations*, to appear (2006).

[2] M. Banda and M. Seaïd, *Higher-Order Relaxation Schemes for Hyperbolic Systems of Conservation Laws*, J. Numer. Math., 13 (2005), pp. 171–196.

[3] M. Banda and M. Seaïd, *Relaxation WENO Schemes for Multi-Dimensional Hyperbolic Systems of Conservation Laws*, preprint.

[4] G. Coclite, M. Garavello and B. Piccoli, *Traffic Flow on Road Networks*, SIAM J. Math. Anal., 36 (2005), pp. 1862–1886.

[5] C. M. Dafermos, *Polygonal Approximations of Solutions of the Initial Value Problem for a Conservation Law*, J. Math. Anal. Appl., 38 (1972), p. 33.

[6] S. Diehl, *A Conservation Law with Point Source and Discontinuous Flux Function*, SIAM J. Math. Anal., 56 (1996), pp. 388–419.

[7] T. Gimse and N.-H. Risebro, *Solution to the Cauchy Problem for a Conservation Law with a Discontinuous Flux Function*, SIAM J. Math. Anal., 23 (1992), pp. 635–648.

[8] G. Lube, L. Müller, and F. C. Otto. A Non-Overlapping Domain Decomposition Method for the Advection-Diffusion Problem. *Computing*, 64(1):49–68, 2000.

[9] H. Holden and N. H. Risebro, *A Mathematical Model of Traffic Flow on a Network of Unidirectional Roads*, SIAM J. Math. Anal., 26 (1995), p. 999–1017.

[10] E. Isaacson and B. Temple, *Analysis of a Singular Hyperbolic System of Conservation Laws*, J. Diff. Equations, 65 (1986), pp. 250–268.

[11] S. Jin and Z. Xin, *The Relaxation Schemes for Systems of Conservation Laws in Arbitrary Space Dimensions*, Comm. Pure Appl. Math., 48 (1995), pp. 235–277.

[12] K. H. Karlsen, C. Klingenberg, and N. H. Risebro, *A Relaxation Scheme for Conservation Laws with Discontinuous Coefficient*, Math. Comp., 73 (2003), pp. 1235–1259.

[13] C. Klingenberg and N. H. Risebro, *Convex Conservation Laws with Discontinuous Coefficients. Existence, Uniqueness and Asymptotic Behaviour*, Comm. Partial Differential Equations, 20 (1995), pp. 1959–1990.

[14] C. Klingenberg and N. H. Risebro, *Stability of a Resonant System of Conservation Laws Modeling Polymer Flow with Gravitation*, J. Differential Equations, 170 (2001), pp. 344–380.

[15] J. E. Lagnese and G. Leugering. *Domain Decomposition Methods in Optimal Control of Partial Differential Equations*, volume 148 of *International Series of Numerical Mathematics*. Birkhäuser Verlag, Basel, 2004.

[16] J. P. Lebacque, *Les Mmodeles Macroscopiques du Traffic*, Annales des Ponts., 67 (1993), pp. 24–45.

[17] M. Lighthill and J. Whitham, *On Kinematic Waves II. A Theory of Traffic Flow on Long Crowded Roads*, Proc. Royal Soc. Edinburgh, A229 (1955), p. 281–345.

[18] J. LeVeque Randall, *Numerical Methods for Conservation Laws*, Lectures in Mathematics ETH Zürich, (1992).

[19] A. Quarteroni and A. Valli. *Domain Decomposition Methods for Partial Differential Equations*. Oxford University Press, Oxford, 1999.

[20] M. Seaïd, *Non-Oscillatory Relaxation Methods for the Shallow Water Equations in One and Two Space Dimensions*, Int. J. Num. Meth. Fluids, 46 (2004), pp. 457–484.

[21] M. Seaïd, *Stable Numerical Methods for Conservation Laws with Discontinuous Flux Function*, Appl. Math. Comput., (2006), in press.

[22] J. D. Towers, *Convergence of a Difference Scheme for Conservation Laws with Discontinuous Flux*, SIAM J. Math. Anal., 38 (2000), pp. 681–698.

[23] P. Zhang and R.-X. Liu, *Generalization of Runge-Kutta Discontinuous Galerkin Method to LWR Traffic Flow Model with Inhomogeneous Road Conditions*, Numer. Methods for PDEs, to appear 21 (2005), pp. 80-88.